

Electronic structure of mixed-valence semiconductors in the LSDA+*U* approximation.

II. SmB₆ and YbB₁₂

V. N. Antonov* and B. N. Harmon
Ames Laboratory, Iowa State University, Ames, Iowa 50011

A. N. Yaresko
Max Planck Institute CPFS, Nöthnitzer Str. 40, D-01187 Dresden, Germany

(Received 12 November 2001; revised manuscript received 14 March 2002; published 8 October 2002)

The electronic structure and optical spectra of SmB₆ and YbB₁₂ are investigated theoretically from first principles, using the fully relativistic Dirac LMTO band structure method. The electronic structure is obtained with the local spin-density approximation (LSDA), as well as with the so-called LSDA+*U* approach. The energy band structures of SmB₆ and YbB₁₂ are related to their measured XPS and UPS spectra as well as optical spectra. The LSDA+*U* band structure calculations produce a small hybridization energy gap in SmB₆ and YbB₁₂ for samarium and ytterbium ions in the divalent state.

DOI: 10.1103/PhysRevB.66.165209

PACS number(s): 71.28.+d, 75.30.Mb

I. INTRODUCTION

SmB₆ and YbB₁₂ are classical mixed valence (MV) narrow gap semiconductors. This class of materials is characterized by their electronic properties, which at high temperatures are associated with a set of independent localized (*f*) moments interacting with a sea of conduction electrons, while at low temperature the electronic properties resemble those of a narrow gap semiconductor. SmB₆ is the first compound in which the phenomena of MV was detected directly by x-ray absorption.¹ Despite more than 35 years of experimental and theoretical effort, many fundamental aspects of the microscopic description of the MV ground state and the nature of valence fluctuations is still under discussion.²⁻⁴ The main problem is the origin of the MV ground state, which seems intimately connected with the gap formation. One question is whether Kondo insulating materials actually are true insulators at low temperatures or whether an intrinsic small conduction-electron carrier concentration is present.⁵ Infrared absorption,⁶ inelastic neutron scattering,⁷ optical conductivity,⁸ electron tunneling,⁹ and electrical transport¹⁰ measurements all detect a small electronic gap, $\Delta = 3-20$ meV. However, the low-temperature transport properties of SmB₆ are manifestly metallic, having a large but finite resistivity below ~ 4 K.¹⁰ There is considerable controversy whether these in-gap states are intrinsic and present in pristine SmB₆,^{7,11,12} or extrinsic and dictated entirely by sample quality.^{10,13} The size of the energy gap determined by different methods varies considerably. For example, the value of the gap in SmB₆ is equal to 2.7 meV by tunneling spectroscopy,⁹ 5 meV from the temperature dependence of the electrical resistivity,¹⁰ and 16 meV by point-contact spectroscopy.¹⁴ Direct measurements of the low-temperature dynamical conductivity and dielectric permittivity of single crystalline SmB₆ give evidence for a 19 meV energy gap and an additional narrow donor-type band lying only 3 meV below the bottom of the upper conduction band.¹⁵

The average valence of Sm in the hexaboride was established to be 2.56 at room temperature, and to vary slightly

with temperature by measurements of x-ray absorption,^{1,16} lattice constant,¹⁷ x-ray photoemission,¹⁸ and Mössbauer isomer shift.¹⁹

YbB₁₂ is thought to be the only known Kondo insulator among Yb compounds with a valence instability. Its physical properties observed near room temperature (metallic conductivity, localized magnetic moments) dramatically change when *T* decreases. At approximately 75 K, the paramagnetic susceptibility goes through a maximum, then decreases rapidly at lower temperatures.²⁰⁻²³ A steep increase in the electrical resistivity is observed in the same temperature range.²⁰⁻²² This, together with the Schottky anomaly in the low-temperature electronic specific heat,^{21,23} provides strong support to the opening of a gap in the electronic excitation spectrum.²⁴ Recent direct optical reflectivity measurements on single crystals of YbB₁₂ also show the opening of an energy gap upon cooling below 70 K.²⁵ The gap development is coincident with a rapid decrease in the magnetic susceptibility, which shows that the gap opening has a significant influence on magnetic properties of YbB₁₂. The energy of the gap, determined by different methods, also varied considerably. Tunneling measurements indicate an energy gap of 200–300 meV,²⁶ the transport gap is much smaller $\Delta \sim 10$ meV,²⁰⁻²² while photoemission measurements reveal gaps of two energy scales:^{27,28} a narrow gap ~ 10 meV and a larger pseudogap of ~ 100 meV. Optical measurements give an energy gap of ~ 25 meV at 20 K.²⁵ It is not yet clear whether the insulating ground state in YbB₁₂ should be ascribed to a “hybridization gap” as predicted in MV models, or reflects the formation of a Kondo singlet on each Yb³⁺ ion. More generally, the influence of the degree of valence mixing on the formation of the Kondo insulator state is not well documented. The Yb valency estimated from the Curie constant below room temperature yields values of about 2.75–2.8 for polycrystals,^{20,21} and 2.95 for a single crystal.²² From the photoemission measurements,²⁷ the valence was estimated to be $\nu = 2.86 \pm 0.06$. X-ray photoelectron spectroscopy (XPS) measurements²⁹ yielded $\nu = 2.9$, whereas the Yb *L*₃ edge x-ray absorption spectrum measured in Ref. 20

was simply denoted “trivalent.” Recent x-ray absorption and inelastic neutron scattering experiments²⁴ indicate that the Yb valence is close to $3+$. On the other hand, the analysis of the magnetic susceptibility together with the Knight shift of YbB_{12} , provided by Wachter,² shows that the susceptibility is zero for $T \rightarrow 0$, in the absence of defects. This might be caused by a nonmagnetic ground state such as $\text{Yb}^{2+} 4f^{14}$ or by a Kondo singlet.

The energy band structures of SmB_6 and YbB_{12} have been calculated by Yanase and Harima³⁰ using the self-consistent LAPW method in the local spin density approximation including the spin-orbit interaction. The LSDA calculations yield a splitting of about 0.05 Ry between the $4f_{5/2}$ and the $4f_{7/2}$ states in SmB_6 . These bands are crossed by the lowest Sm 5d band. It was found that a small direct energy gap of around 14 meV exists at the Fermi energy along the Δ -axis. LSDA calculations generally provide an inadequate description of the 4f electrons due to improper treatment of correlation effects. In particular, LSDA calculations cannot account for the splitting of filled and empty f bands (determined, for example, by photoemission and BIS experiments), which is expected to be 7–8 eV in SmB_6 and YbB_{12} .¹⁸

The previous paper³¹ is devoted to the theoretical investigation of the electronic structure and optical spectra of samarium monochalcogenides. The aim of this work is the theoretical study of the electronic structure and optical spectra of the mixed valent semiconductors SmB_6 , and YbB_{12} . While there are difficulties in describing the MV states using the LSDA and LSDA+ U methods, it is important to establish how well these methods can describe features of the electronic structure, and which features will require more sophisticated many-body treatments. To help separate MV effects, we also investigate theoretically the electronic structure and optical spectra of LuB_{12} as a reference compound. The description of the computational details have been presented in the previous paper.³¹

This paper is organized as follows: Sec. II is devoted to the electronic structure and optical properties of the SmB_6 , YbB_{12} , and LuB_{12} calculated in the LSDA and LSDA+ U approximations. The theoretical calculations of XPS and optical spectra are also compared to the experimental measurements. Finally, the results are summarized in Sec. III.

II. RESULTS AND DISCUSSION

A. SmB_6

The compound SmB_6 has the CaB_6 type crystal structure with space group $Pn3m$ (No. 221) and lattice constant equal to 4.1333 Å.³² The structure of samarium hexaboride may be viewed as a CsCl-type lattice with the cesium replaced by samarium and the chlorine by a B_6 octahedron. Figure 1 shows the energy band structure of SmB_6 calculated within the LSDA and the LSDA+ U approximations. The energy band structure of SmB_6 with the LSDA approximation can be subdivided into three regions separated by energy gaps. The bands in the lowest region around -14 to -16 eV (not shown) have mostly B 2s character with some amount of Sm

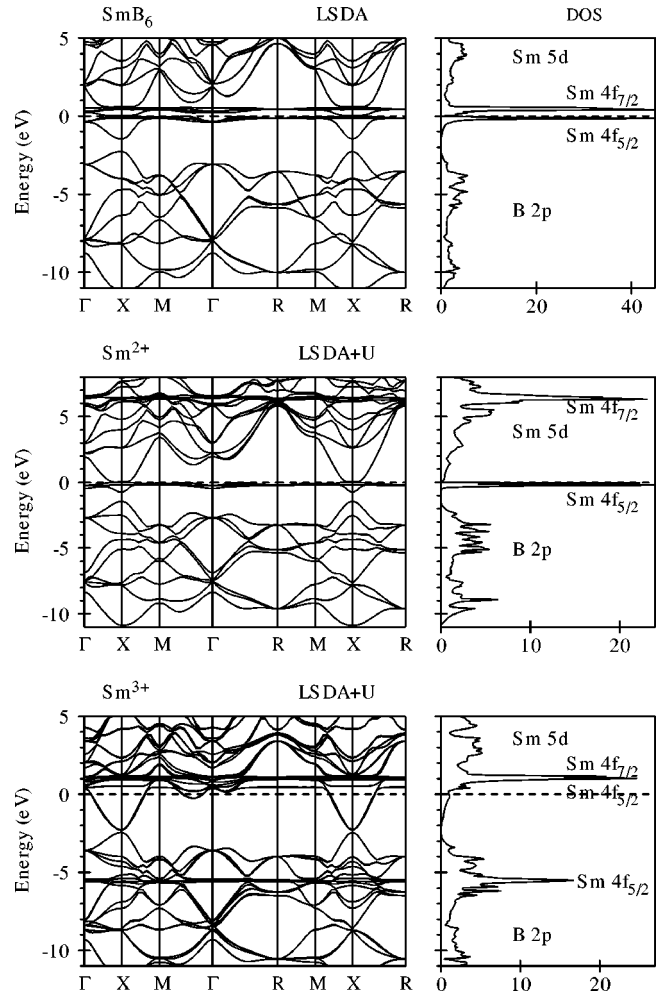


FIG. 1. Self-consistent fully relativistic, spin-polarized energy band structure and total DOS [in states/(unit cell eV)] calculated for SmB_6 with the LSDA and LSDA+ U approximations.

sp character mixed in. The next group of energy bands are B 2p bands separated from the 2s bands by an energy gap of about 3 eV. The width of the B 2p band is about 8.8 eV. The Sm 5d bands are partly occupied. They are also separated from B 2p states by the energy gap of around 0.7 eV. The sharp peaks in the DOS calculated in the LSDA just below and above the Fermi energy are due to $4f_{5/2}$ and $4f_{7/2}$ states, respectively (Fig. 1). They cross the Sm 5d bands and hybridize with them. There is a small direct energy gap at the Fermi level of around 23 meV. Our LSDA band structure of SmB_6 is in good agreement with previous calculations of Yanase and Harima.³⁰

The LSDA+ U energy bands and total density of states (DOS) of SmB_6 for $U_{\text{eff}}=7$ eV are shown in Fig. 1. The Coulomb repulsion U_{eff} strongly influences the electronic structure of SmB_6 . For Sm^{3+} ions five $4f_{5/2}$ bands are fully occupied and hybridized with the B 2p states. The $4f_{7/2}$ unoccupied states are above the Fermi level at around 1 eV. A single $4f_{5/2}$ level is fully unoccupied and situated at about 0.34 eV above the Fermi level.

In our LSDA+ U band structure calculations we started from a $4f^6$ configuration for the Sm^{2+} ion with six on-site

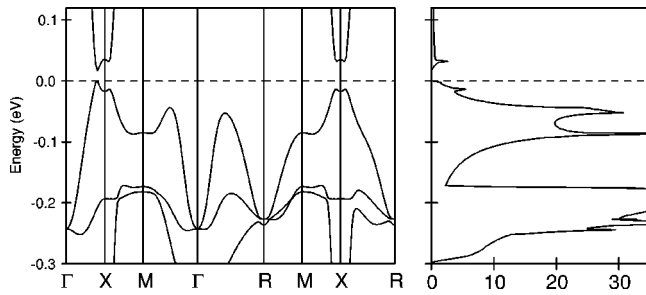


FIG. 2. Expanded view of the energy band structure and total DOS [in states/(unit cell eV)] of SmB_6 for Sm^{2+} ions calculated in the $\text{LSDA}+U$ approximations.

$4f$ energies shifted downward by $U_{\text{eff}}/2$ and eight levels shifted upwards by this amount. The energies of occupied $4f_{5/2}$ and unoccupied $4f_{7/2}$ levels are separated by approximately U_{eff} (Fig. 1). For Sm^{2+} ions, eight $4f_{7/2}$ hole levels are completely unoccupied and well above the Fermi level and hybridized with $\text{Sm } 5d$ states. The $4f_{5/2}$ bands are situated in close vicinity of the Fermi level. They cross the bottom of the $\text{Sm } 5d$ band. Figure 2 shows an expanded view of the $\text{LSDA}+U$ energy band structure and total DOS for SmB_6 with Sm^{2+} ions. There is a hybridization gap at the Fermi level $\Delta E = 27$ meV. Although we used a starting configuration with fully occupied $4f_{5/2}$ bands, in the process of self-consistent relaxation one of the $4f_{5/2}$ doubly degenerate bands becomes partly unoccupied and situated above the Fermi level around the X symmetry point (Fig. 2) due to $\text{Sm } 5d-4f$ hybridization. There is a small peak in the DOS above the Fermi level at around 0.03 eV with predominantly $4f$ character (to produce this fine structure we increased the number of \mathbf{k} points in the irreducible part of the Brillouin zone up to 8125). This peak contains 0.02 $4f$ holes. In other words, our $\text{LSDA}+U$ calculations produce a semiconducting ground state in SmB_6 with a noninteger Sm valency equal to $2.02+$.

The ground state of an intermediate valence compound is a quantum mechanical mixture of both the $4f^n$ and the $4f^{n-1}5d$ configuration on each rare earth ion. Such compounds need theoretical consideration beyond the mean field one-particle $\text{LSDA}+U$ approximation due to possible configuration interaction between different $4f$ valence states. It can lead to spontaneous interconfiguration fluctuations (ICF), introduced first by Hirst.³³ As briefly discussed by Varma,³⁴ at $T=0$, “fluctuations” can be either static or dynamic. In the static case the system is spatially “inhomogeneous” in the sense that at inequivalent sites different valence states are present. Examples among the rare earth compounds are Eu_3S_4 , Eu_3O_4 ,¹⁸ and the charge ordering heavy fermion Yb_4As_3 compound.³⁵ Such static charge “fluctuations” have been known for a long time in the $3d$ -series; Fe_3O_4 , magnetite, being a typical example (see Ref. 36, and references therein). In the dynamic case the system shows fast local fluctuations which give an intrinsic width to the f -levels. At any given site $4f$ charge fluctuations between the two configurations occur on a time scale τ_{ICF} , the so called *interconfiguration fluctuation time*.³⁷ The system on time average is “homogeneous,” i.e., all sites are equivalent. Experiments

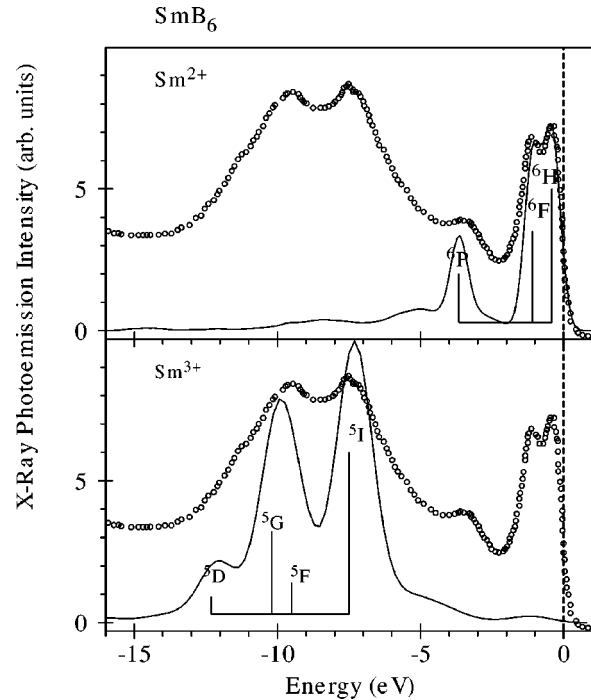


FIG. 3. Comparison of the calculated $4f$ DOS of SmB_6 using the $\text{LSDA}+U$ approximation with the experimental XPS spectra from Ref. 18, taking into account the multiplet structure of the $4f^5$ and $4f^4$ final states (see explanations in the text).

such as lattice constant and isomer shift measurements, which probe the sample on a time scale much longer than τ_{ICF} , will see only one intermediate configuration, but experiments such as XPS or UPS measurements which take place in a time much shorter than τ_{ICF} (up to 10^6-10^7 times shorter) will see the instantaneous picture of a mixture of the ions in the two valence states.

The XPS spectra for SmB_6 indicate a multiplet structure which can be identified with both Sm^{2+} and Sm^{3+} configurations being present. Figure 3 shows the SmB_6 XPS spectrum¹⁸ in comparison to the occupied part of the partial $\text{LSDA}+U$ $4f$ DOS calculated with a multiplet structure of the final states taken into account in the same way as for SmS and $\text{Sm}_{0.5}\text{Th}_{0.5}\text{S}$ in our previous paper³¹ (i.e., we calculated atomic multiplet structures for Sm^{2+} and Sm^{3+} ions and positioned their centroid with the centroid of the $\text{LSDA}+U$ occupied $4f$ DOS peaks calculated for the Sm^{2+} and Sm^{3+} configurations shown in Fig. 1). We show in Fig. 3 the final state multiplet structure presented in Ref. 18. Sm^{2+} ($4f^5$ final state) has the multiplets ^6H , ^6F , and ^6P . Sm^{3+} ($4f^4$ final state) has the multiplets ^5I , ^5F , ^5G , and ^5D .¹⁸ It is clear that the structures between 0.0 and -5.5 eV binding energy should be assigned to the final-state multiplet structure derived from six fully occupied $4f$ bands (Sm^{2+}) and the structures between -5.5 and -13 eV are associated with the final state multiplet structure of the Sm^{3+} ions. The agreement with the positions of the multiplet peaks indicates that the $\text{LSDA}+U$ is giving reasonably correct average positions for the occupied $4f$ states.

Let us turn now to the optical properties of SmB_6 . Experimental investigation of the reflectivity spectra of SmB_6

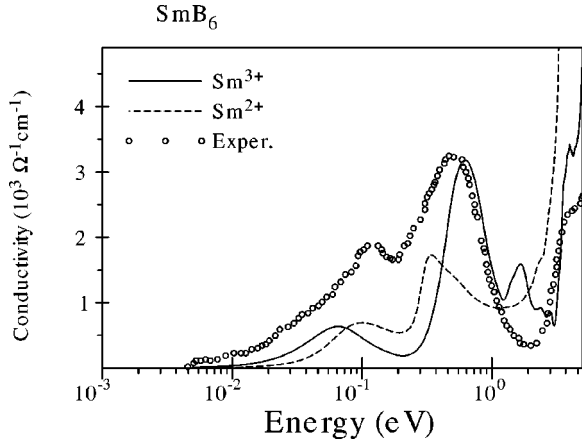


FIG. 4. Calculated diagonal part of the optical conductivity $\sigma_{1,xx}(\omega)$ of SmB_6 in the LSDA+ U approximation compared with the experimental measurements at 13 K (open circles) (Ref. 41).

was performed by Kierzek-Pecold³⁸ in a narrow energy range from 1 to 5.6 eV. After that, Travaglini and Wachter measured the reflectivity spectrum of SmB_6 in the energy range from 1 meV to 12 eV at 300 K and 4 K for investigation of the energy gap.⁸ Kimura and co-workers measured the optical spectra of all single crystal rare-earth hexaborides RB_6 ($R=\text{La, Ce, Pr, Nd, Sm, Eu, Gd, Th, Dy, Ho, Yb, and Y}$) in the energy region from 1 meV to 40 eV at 300 K and 13 K.^{39–42}

Figure 4 shows with a logarithmic scale the calculated optical conductivity spectra of SmB_6 compared with experimental data measured at 13 K.⁴¹ Calculations were performed for both the divalent and trivalent phases of SmB_6 . The experimentally measured optical conductivity spectrum has two strong peaks at 0.12 and 0.5 eV and a steep rise at 3 eV (Fig. 4). As might be expected, the experimental optical conductivity spectrum contains key features of both the divalent and trivalent theoretically calculated spectra. However, the three major peaks have different origins in the divalent and trivalent phases. A steep increase of optical conductivity starting at around 3 eV is mostly determined by $\text{B } 2p \rightarrow \text{Sm } 5d$ interband transitions around the X symmetry point in the divalent samarium compound. The same feature in the trivalent phase can be described as a combination of the $\text{B } 2p \rightarrow \text{Sm } 5d$ and $\text{Sm } 5d \rightarrow \text{Sm } 4f$ interband transitions. These transitions also occur mostly around the X symmetry point (Fig. 1). The low energy peak at 0.12 eV in the divalent phase can be explained as interband transitions between occupied $\text{Sm } d-f$ mixed states and unoccupied $\text{Sm } 5d$ states near the X symmetry point. The same structure in the trivalent Sm phase is due to interband transitions among hybridized $\text{Sm } 5d$ bands along $\Gamma-X$, $\Gamma-M$, $X-M$, and $X-R$ symmetry directions. This peak is shifted at around 0.1 eV toward smaller energies in comparison with the experimental measurements. The peak at 0.5 eV in the divalent phase arises from interband transitions between occupied $\text{Sm } d-f$ mixed states and unoccupied $\text{Sm } 5d$ states near the X symmetry point and $\Gamma-X$ and $X-M$ symmetry directions. The same structure in the trivalent samarium phase is due to in-

terband transitions between occupied $\text{Sm } 5d$ states and the empty 6th $4f$ hole band along $\Gamma-X$, $\Gamma-M$, and $X-M$ symmetry directions.

As we mentioned above, the XPS measurements cannot distinguish between an inhomogeneously mixed or a homogeneously mixed compound, i.e., whether Sm^{2+} and Sm^{3+} ions are integer valent and statically mixed or the charge between them just fluctuates slower than the time resolution of XPS. The experimental optical conductivity spectrum also can be considered as a mixture of both the divalent and trivalent spectra. From other experiments, SmB_6 is known to be a homogeneous mixed-valence semiconductor compound with a small energy gap.² Mössbauer isomer shift vs temperature measurements for SmB_6 by Cohen *et al.* clearly show that above 700 K and down to 4.2 K, the degree of valence mixing is a constant of around 2.56.¹⁹ Our LSDA+ U band structure calculations produce a metallic state with trivalent samarium ions if we start our self-consistent procedure from Sm^{3+} . On the other hand, if we used as starting configuration with fully occupied $4f_{5/2}$ levels (Sm^{2+}), we are able to produce a correct semiconductor ground state for SmB_6 with a small hybridization energy gap, and a theoretically calculated valency 2.02+. A comprehensive theory for the MV state is needed to provide a quantitative measure of the mixing between the two configurational states. Our calculations are only able to provide specific details for the individual configurational states.

B. YbB_{12}

The compound YbB_{12} has the UB_{12} type crystal structure with space group $Fm\bar{3}m$ (No. 225) and lattice constant equal to 7.464 Å.³² The crystal structure of YbB_{12} can be understood as a fcc NaCl type with the sodium replaced by ytterbium and the chlorine by 12 B atoms.

In our band structure calculations we have performed three independent fully relativistic spin-polarized calculations. We consider the $4f$ electrons as (1) itinerant electrons using the local spin-density approximation; (2) fully localized, putting them in the core; and (3) partly localized using the LSDA+ U approximation. Figure 5 shows the energy band structure of YbB_{12} for all three approximations. The energy band structure of YbB_{12} with $4f$ electrons in the core can be subdivided into three regions. The bands in the lowest region around -15.5 to -10 eV have mostly B $2s$ character with some amount of Yb sp character mixed in. The next group of the energy bands are B $2p$ bands separated from the $2s$ bands by a small energy gap of about 0.4 eV. The width of the B $2p$ band is about 8 eV. The Yb $5d$ bands are partly occupied and cross the Fermi energy. They slightly overlap with B $2p$ states. The sharp peaks in the DOS calculated in the LSDA just below the Fermi energy are due to Yb $4f_{5/2}$ and $4f_{7/2}$ states (Fig. 5). They cross Yb $5d$ bands and hybridize with them. There is a small direct energy gap of about 65 meV at the Fermi level. Our LSDA band structure of YbB_{12} is in good agreement with previous calculations of Yanase and Harima except that the latter authors found YbB_{12} to be a semimetal.³⁰

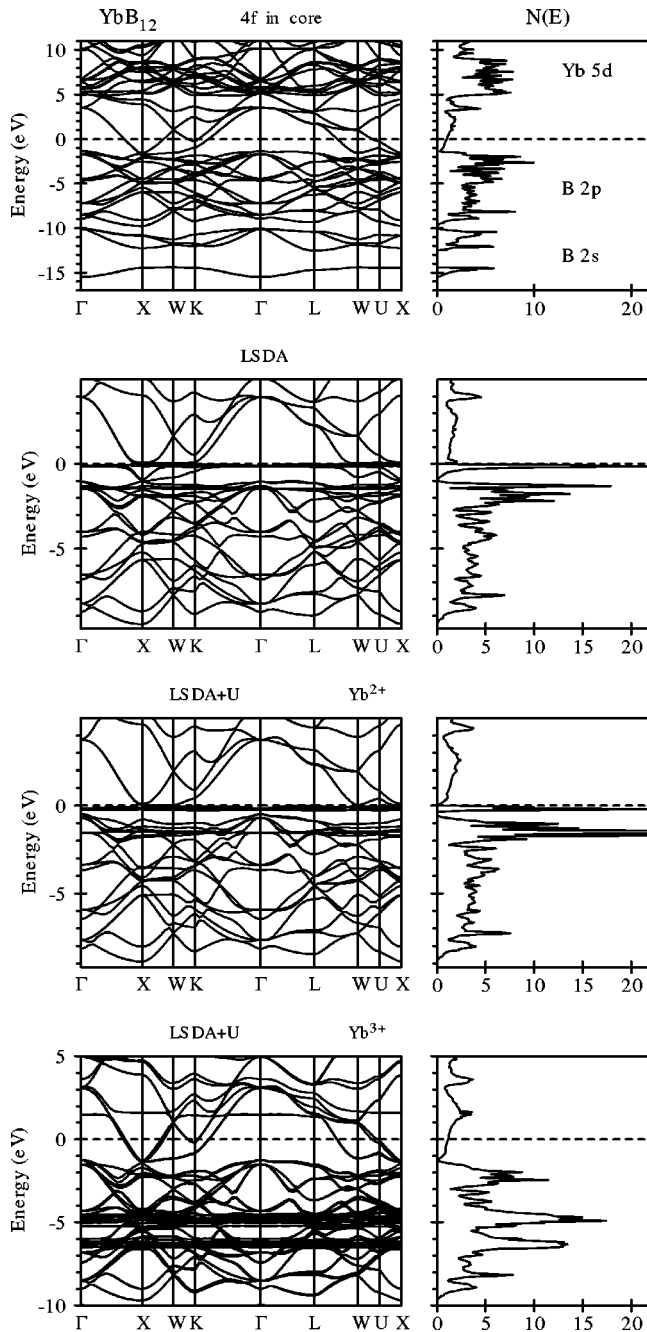


FIG. 5. Self-consistent fully relativistic, spin-polarized energy band structure and total DOS [in states/(unit cell eV)] calculated for YbB_{12} with the LSDA and LSDA+ U approximations.

The LSDA+ U energy bands and total density of states of YbB_{12} for $U_{\text{eff}}=8$ eV are shown in Fig. 5. We start the self-consistent calculations from the $4f^{14}$ configuration for the Yb^{2+} ion, where all 14 on-site $4f$ energies are shifted downwards by $U_{\text{eff}}/2$, and from the $4f^{13}$ configuration for the Yb^{3+} ion with 13 on-site $4f$ energies are shifted downwards by $U_{\text{eff}}/2$ and one level shifted upwards by this amount. The energies of occupied and unoccupied Yb^{3+} f bands are separated by approximately U_{eff} .

For divalent Yb ions all 14 $4f$ bands are fully occupied and situated closely below the bottom of the Yb d band.

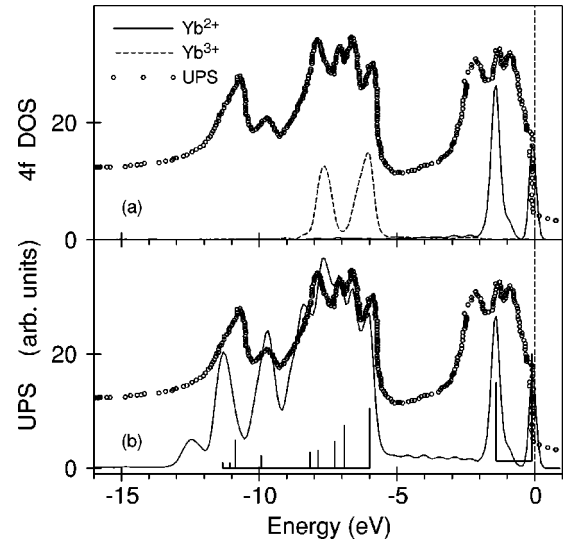


FIG. 6. (a) The calculated $4f$ DOS of YbB_{12} for Yb^{2+} and Yb^{3+} configurations in comparison to the experimental UPS spectra from Ref. 26; (b) the calculated $4f$ DOS of YbB_{12} taking into account the multiplet structure of the $4f^{13}$ and $4f^{12}$ final states (see explanation in the text) in comparison to the experimental UPS spectra from Ref. 26.

They are split due to spin-orbit coupling by $\Delta\varepsilon_{\text{so}}=1.4$ eV. There is a small hybridization gap at the Fermi level. In other words, the calculations indicate a nonmagnetic semiconducting ground state in YbB_{12} for Yb atoms in the divalent state. The theoretically calculated energy gap, $\Delta E=65$ meV, is formed between Yb $4f_{7/2}$ and Yb $5d$ states. The experimentally estimated energy gap is about 10 meV from the activation energy,^{20–22} 25 meV from optical measurements²⁸ and 200–300 meV from tunneling experiments.²⁵

For the trivalent Yb ion, thirteen $4f$ electron bands are well below the Fermi energy and hybridized with the B $2p$ states (Fig. 5). The 14th $4f$ unoccupied hole level is above the Fermi level at around 1.5 eV. We should mention that such an electronic structure is appropriate for the development of the Kondo scenario.^{43–45}

The partial $4f$ DOS of the occupied part of YbB_{12} calculated in the LSDA+ U approximation is compared with ultraviolet photoelectron spectra (UPS) (Refs. 26, 27) in Fig. 6. The experimental spectra were measured using both single crystalline²⁶ and polycrystalline²⁷ samples. The double peak structure at 0.1 and 1.5 eV binding energy reflects the spin-orbit doublet of the Yb^{2+} density of states. The corresponding spin-orbit doublet for the Yb^{3+} DOS is situated at -6.0 and -7.6 eV [Fig. 6(a)].

Calculated $4f$ DOS cannot, of course, fully account for the multiplet splitting. Therefore we present in Fig. 6(b) the $4f$ DOS's taking into account the multiplet structure in the same way as for SmB_6 . We used the theoretical final state multiplet structure presented in Ref. 37. Yb^{2+} has the configuration $4f^{14}$. The $n-1$ state $4f$ (Ref. 13) has one hole in the $4f$ shell and cannot reproduce the experimentally measured four peak structure in the XPS. One would expect only

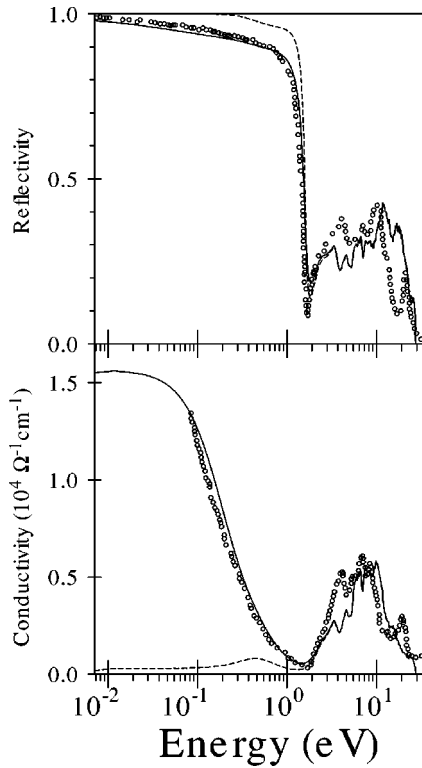


FIG. 7. Calculated optical reflectivity $R(\omega)$ and diagonal part of the optical conductivity $\sigma_{1,xx}(\omega)$, of LuB_{12} in the LSDA approximation: dashed line without and solid line with the Drude term compared with the experimental data (open circles) (Ref. 28). Above ~ 1 eV the dashed and solid lines coincide.

the spin-orbit doublet, and the 4 peak structure is almost certainly due to surface effects.⁴⁶

After consideration of the band structure and UPS spectra of YbB_{12} , we turn to the optical spectra. Recently optical reflectivity experiments have been conducted by Okamura *et al.* on single crystals of YbB_{12} .²⁸ They found that upon cooling below 70 K, a strong suppression of the optical conductivity $\sigma(\omega)$ was seen in the far-infrared region, reflecting the opening of an energy gap of ~ 25 meV. A narrow, asymmetric peak was observed at ~ 40 meV in $\sigma(\omega)$, which was attributed to optical transitions between the Yb $4f$ -derived states across the gap.²⁸ They also measured the optical spectra of single crystalline LuB_{12} as a reference material.

Figure 7 shows with a logarithmic scale the calculated optical reflectivity $R(\omega)$ and diagonal part of optical conductivity $\sigma_{1,xx}(\omega)$ spectra of LuB_{12} compared with the experimental data.²⁸ We mention, furthermore, that we have convoluted the calculated spectra with a Lorentzian whose width is 0.2 eV to approximate lifetime broadening. To incorporate the intraband contribution to the optical conductivity tensor we use the phenomenological Drude model⁴⁵ with intraband Drude relaxation time $\gamma_D = 0.3$ eV. A sharp onset is seen in the LuB_{12} reflectivity spectrum $R(\omega)$ near 1.6 eV, which can be identified as the plasma edge (ω_p) due to a metallic response of free carriers. The peak structures above ω_p are due to interband transitions between electronic states far apart from E_F . Figure 7 clearly shows the important role of intraband transitions in the formation of the optical conductivity spectrum in LuB_{12} .

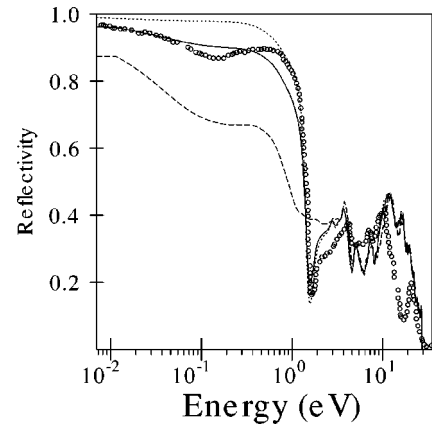


FIG. 8. The experimental optical reflectivity spectrum $R(\omega)$ of YbB_{12} (open circles) measured at 290 K (Ref. 28) in comparison with theoretical calculations in the LSDA+ U approximation: dotted line for Yb^{3+} , dashed line for Yb^{2+} ions, and solid line for $R = 0.2 * R^{2+} + 0.8 * R^{3+}$.

Figure 8 shows the calculated optical reflectivity spectra of YbB_{12} compared with experimental data measured at 290 K.²⁸ Calculations were performed for both the divalent and trivalent phases of YbB_{12} . We also included the intraband optical transitions in Drude form with inverse intraband Drude relaxation time $\gamma_D = 0.1$ eV.

The optical reflectivity spectrum of YbB_{12} measured at 290 K has a metallic character, very similar to LuB_{12} $R(\omega)$ with the same plasma edge at 1.6 eV. The two spectra are almost identical for the energy interval above ω_p . Below ω_p , in contrast, the spectra are strictly different for the two compounds. In LuB_{12} , $R(\omega)$ is nearly flat and $\sigma(\omega)$ shows a sharp rise, which is typical of a good metal, while in YbB_{12} there is a broad dip in $R(\omega)$ giving rise to a prominent peak at 0.25 eV in $\sigma(\omega)$. As can be seen from Fig. 8 a broad dip in $R(\omega)$ comes from YbB_{12} with divalent Yb ions. Our LSDA+ U calculations produce the reflectivity spectrum in YbB_{12} with trivalent ytterbium ions very similar to the LuB_{12} spectrum. The experimentally measured optical reflectivity spectrum of YbB_{12} can be considered as a mixture of two spectra coming from di- and trivalent ytterbium ions. Good agreement between theory and experiment can be reached if one uses the sum of the optical reflectivity spectrum consisting of 20% ytterbium divalent and 80% ytterbium trivalent spectra (Fig. 8).

The experimental investigations of the temperature dependence of the optical spectra of YbB_{12} presented in Ref. 28 show that as the temperature is lowered from 290 K to 78 K, there is no drastic change in the optical conductivity spectrum. The IR peak becomes slightly enhanced and blue-shifted. At 78 K the spectra are still metallic. However, at 20 K the spectral weight below ~ 40 meV in $\sigma(\omega)$ is strongly depleted and the spectrum becomes typical of a semiconductor with an energy gap of around 25 meV. The reflectivity spectrum at 20 K is also typical of a semiconductor having the asymptotic value at $\omega \rightarrow 0$ of 0.83. The gap development coincides with the rapid decrease of the magnetic susceptibility in exactly the same temperature range.²⁸

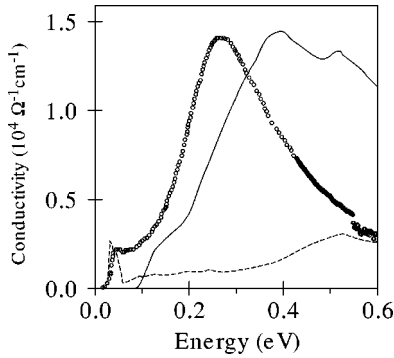


FIG. 9. Calculated diagonal part of the optical conductivity $\sigma_{1,xx}$, of YbB_{12} in the LSDA+ U approximation for the Yb^{2+} ion (full line) and Yb^{3+} ion (dashed line) compared with the experimental data (open circles) (Ref. 28).

Figure 9 shows the calculated diagonal part of optical conductivity $\sigma_{1,xx}(\omega)$ spectra of YbB_{12} compared with experimental data.²⁸ Calculations were performed for both the divalent and trivalent phases of YbB_{12} . The experimentally measured optical conductivity spectrum in the 0–0.6 eV energy interval has two peaks at 0.05 and 0.25 eV (Fig. 9). The experimental optical conductivity spectrum of YbB_{12} contains key features of both the divalent and trivalent theoretically calculated spectra. The low energy peak at 0.05 eV in the optical conductivity spectrum originates from the trivalent phase and can be explained as interband transitions between occupied and unoccupied Sm 5*d* states along Γ – X and X – W symmetry directions (Fig. 5). The prominent peak in $\sigma_{1,xx}(\omega)$ spectrum at around 0.4 eV (the corresponding experimental peak situated at 0.25 eV) is mostly derived from the interband transitions between occupied Yb 4*f* bands and empty Yb 5*d* bands of divalent phase in the vicinity of the W symmetry point as well as along the X – W symmetry direction (Fig. 5). The theoretically calculated $\sigma_{1,xx}(\omega)$ spectrum in the divalent phase is shifted toward higher energies due to the larger theoretically calculated energy gap (65 meV) in comparison to the experimental one (25 meV).

III. SUMMARY

Classical mixed valence narrow gap semiconductors SmB_6 and YbB_{12} constitute very interesting systems exhibiting behavior due to strongly correlated electrons. The LSDA calculations provide an inadequate description of the 4*f* electrons in SmB_6 and YbB_{12} due to improper treatment of the correlation effects.

The Coulomb repulsion U_{eff} strongly influences the electronic structure of SmB_6 . For Sm^{2+} ions eight 4*f*_{7/2} hole levels are completely unoccupied and well above the Fermi level hybridized with Sm 5*d* states. The 4*f*_{5/2} bands are situated in close vicinity of the Fermi level. One of the 4*f*_{5/2} levels is slightly unoccupied and extends just above the Fermi level around the X symmetry point, producing a non-integer Sm valency equal to 2.02+. There is a small hybridization gap at the Fermi level, $\Delta E = 27$ meV. The theoret-

cally calculated energy gap is larger than the experimentally estimated one of around 3.6–5.2 meV, determined from the activation energy and optical measurements. For Sm^{3+} five 4*f* bands are fully occupied and situated at around 6 eV below the Fermi level. A 6th 4*f* hole level is fully unoccupied and situated at about 0.34 eV above the Fermi level. The average positions of the occupied 4*f* states in Sm^{2+} and Sm^{3+} calculations are in agreement with XPS measurements.

In the LSDA+ U energy band structure calculations of the electronic structure of YbB_{12} with divalent Yb ions all 14 4*f* bands are fully occupied and situated closely below the bottom of the Yb 5*d* band. They are split due to spin–orbit coupling by $\Delta\varepsilon_{\text{so}} = 1.4$ eV. There is a small hybridization gap at the Fermi level. The theoretically calculated energy gap, $\Delta E = 65$ meV between Yb 4*f*_{7/2} and Yb 5*d* states, is somewhat larger than the gap estimated from the activation energy and optical measurements and smaller than observed in tunneling experiments. For the trivalent Yb ion, thirteen 4*f* electron bands are well below the Fermi level and hybridized with the B 2*p* states. They are separated from a 4*f* hole state by the correlation energy U_{eff} . The 14th 4*f* unoccupied hole level is well above the Fermi level at around 1.5 eV.

The optical spectra of YbB_{12} can be considered as a mixture of two spectra coming from di- and trivalent ytterbium ions. Good agreement between theory and high temperature optical reflectivity spectrum can be reached if one uses the sum of the optical reflectivity spectrum consisting of 20% ytterbium divalent and 80% ytterbium trivalent spectra. Low temperature measurements show that below 20 K there is a gap development in the optical conductivity and reflectivity spectra of YbB_{12} . The low energy peak at 0.05 eV in the optical conductivity spectrum originates from the trivalent phase and can be explained as interband transitions between occupied and unoccupied Sm 5*d* states along Γ – X and X – W symmetry directions. The prominent peak in the $\sigma_{1,xx}(\omega)$ spectrum at around 0.4 eV is mostly derived from interband transitions between occupied Yb 4*f* bands and empty Yb 5*d* bands of the divalent phase in the vicinity of the W symmetry point as well as along the X – W symmetry direction.

We should mention that the situation in YbB_{12} is still vague both experimentally and theoretically, and that more experimental data may help clarify the picture. If ytterbium in this compound is practically trivalent, as claimed based on recent measurements of x-ray absorption and inelastic neutron-scattering by Alekseev *et al.*,²⁴ then the gap in the tunneling and other experiments could be ascribed only to a Kondo insulator (KI) state. However, it is difficult to understand this. The necessary precondition for the KI state is a nearly half-filled single conduction band, but the LSDA+ U band structure calculations with Yb^{3+} ions produce several sheets of Fermi surface (see the lowest panel of Fig. 5). The influence of the degree of valence mixing on the formation of the Kondo insulator state in YbB_{12} will require further theoretical and experimental investigations.

In conclusion, we would like to point out that the LSDA+ U method which combines LSDA with a basically static,

i.e., Hartree-Fock-type, mean-field approximation for a multiband Anderson lattice model does not contain true many-body physics. However, this method can be considered as the first step towards a better description of strongly correlated electron systems. The LSDA+ U method gives a correct insulating ground state solution for Sm monochalcogenides at ambient pressure. This method provides the correct energy positions of $4f$ energy bands and gives a reasonable description of the optical properties in Sm X ($X = S, Se, Te$), SmB $_6$, and YbB $_{12}$. However, the paramagnetic phase of the high pressure SmS golden phase as well as the formation of the MV state in SmB $_6$ and YbB $_{12}$ clearly requires a treatment that goes beyond a static mean-field

approximation and includes dynamical effects, e.g., the frequency dependence of the self-energy.

ACKNOWLEDGMENTS

This work was carried out at the Ames Laboratory, which is operated for the U.S. Department of Energy by Iowa State University under Contract No. W-7405-82. This work was supported by the Director for Energy Research, Office of Basic Energy Sciences of the U.S. Department of Energy. V.N. Antonov gratefully acknowledges the hospitality at Ames Laboratory during his stay. The authors are very grateful to Professor K. Kikoin for reading the manuscript and for fruitful discussions.

*Permanent address: Institute of Metal Physics, 36 Vernadskii Street, 252142 Kiev, Ukraine.

¹E. E. Vanstein, S. M. Blokhin, and Yu. B. Paderno, *Sov. Phys. Solid State* **6**, 281 (1965).

²P. Wachter, *Handbook of the Physics and Chemistry of Rare Earths*, edited by K. A. Gschneidner, Jr., L. Eyring, and S. Hufner (North-Holland, Amsterdam, 1994), Vol. 19, p. 177.

³P. S. Riseborough, *Adv. Phys.* **49**, 257 (2000).

⁴L. Degiorgi, *Rev. Mod. Phys.* **71**, 687 (1999).

⁵Z. Fisk, J. L. Sarrao, S. L. Cooper, P. Nyhus, G. S. Boehinger, A. Passner, and P. C. Canfield, *Physica B* **223-224**, 409 (1996).

⁶S. von Molnar, T. Theis, A. Benoit, A. Briggs, J. Floquet, J. Ravex, and Z. Fisk, in *Valence Instabilities*, edited by P. Wachter and H. Boppart (North-Holland, Amsterdam, 1982), p. 389; T. Nanba, H. Ohta, M. Motokawa, S. Kimura, S. Kunil, and T. Kasuya, *Physica B* **186-188**, 440 (1993).

⁷P. A. Alekseev, V. A. Lazukov, R. Osborn, B. D. Rainford, I. P. Sadikov, E. S. Konovalova, and Yu. B. Paderno, *Europhys. Lett.* **23**, 347 (1993); J.-M. Mignot, P. A. Alekseev, J. Rossat-Mignot, V. N. Lazukov, and I. P. Sadikov, *Physica B* **199-200**, 430 (1994); P. A. Alekseev, J.-M. Mignot, J. Rossat-Mignot, V. N. Lazukov, I. P. Sadikov, E. S. Konovalova, and Yu. B. Paderno, *J. Phys.: Condens. Matter* **7**, 289 (1995); J.-M. Mignot and P. A. Alekseev, *Physica B* **215**, 99 (1995).

⁸G. Travaglini and P. Wachter, *Phys. Rev. B* **29**, 893 (1984).

⁹B. Battlog, P. H. Schmidt, and J. M. Rowwel, in *Valence Fluctuations in Solids*, edited by L. M. Falikov, W. Hunke, and M. B. Maple (North-Holland, Amsterdam, 1981), p. 357; L. Frankowski and P. Wachter, *Solid State Commun.* **41**, 577 (1982).

¹⁰A. Menth, E. Buetler, and T. H. Geballe, *Phys. Rev. Lett.* **22**, 295 (1969); J. C. Nickerson, R. M. White, K. N. Lee, R. Bachmann, T. H. Geballe, and G. W. Hull, *Phys. Rev. B* **3**, 2030 (1971); J. W. Allen, B. Batlogg, and P. Wachter, *ibid.* **20**, 4807 (1979).

¹¹J. C. Cooley, M. C. Aronson, Z. Fisk, and P. C. Canfield, *Phys. Rev. Lett.* **74**, 1629 (1995).

¹²T. Kasuya, K. Takegahara, T. Fujita, T. Tanaka, and E. Bannai, *J. Phys. Colloq.* **40**, C5-308 (1979).

¹³J. Morillo, G. Bordier, C. H. de Novion, J. P. Senateur, and J. Jun, *J. Magn. Magn. Mater.* **47-48**, 465 (1985); T. H. Geballe, A. Menth, E. Buehler, and G. W. Hall, *J. Appl. Phys.* **41**, 904 (1979).

¹⁴S. Koni, *J. Magn. Magn. Mater.* **63-64**, 673 (1987).

¹⁵B. Gorshunov, N. Sluchanko, A. Volkov, M. Dressel, G. Krebel,

A. Loidl, and S. Koni, *Phys. Rev. B* **59**, 1808 (1999).

¹⁶J. M. Taraskon, Y. Ishikawa, B. Chevalier, J. Etourneau, P. Hagemuller, and M. Kasuya, *J. Phys. (Paris)* **41**, 1141 (1980).

¹⁷T. Kasuya, M. Kasaya, K. Takegahara, T. Fujita, T. Goto, A. Tamaki, M. Takigawa, and H. Yasuoka, *J. Magn. Magn. Mater.* **31-34**, 447 (1983).

¹⁸M. Campagna, G. K. Wertheim, and E. Bucher, *Structure and Bonding* (Springer, Berlin, 1976), Vol. 30, p. 99.

¹⁹R. L. Cohen, M. Eibschutz, K. W. West, and E. Buller, *J. Appl. Phys.* **41**, 898 (1970).

²⁰M. Kasuya, F. Iga, K. Negishi, S. Nakai, and T. Kasuya, *J. Magn. Magn. Mater.* **31-34**, 437 (1983).

²¹M. Kasuya, F. Iga, M. Takigawa, and T. Kasuya, *J. Magn. Magn. Mater.* **47-48**, 429 (1985).

²²F. Iga, N. Shimizu, and T. Takabatake, *J. Magn. Magn. Mater.* **177-181**, 337 (1998).

²³F. Iga, S. Hura, J. Kljcin, N. Shimizu, T. Takabatake, M. Ito, Y. Matsumoto, F. Masaki, T. Suzuki, and T. Fujita, *Physica B* **259-261**, 312 (1999).

²⁴P. A. Alekseev, E. V. Nefeodova, U. Straub, J.-M. Mignot, V. N. Lazukov, I. P. Sadikov, L. Soderholm, S. R. Wassermann, Yu. B. Paderno, N. Yu. Shitsevalova, and A. Murani, *Phys. Rev. B* **63**, 064 411 (2001).

²⁵T. Ekino, H. Umeda, F. Iga, N. Shizu, T. Tahabatake, and H. Fujii, *Physica B* **259-261**, 315 (1999).

²⁶T. Susaki, Y. Takeda, M. Arita, K. Mamiya, A. Fujimori, K. Shimada, H. Namatame, M. Taniguchi, N. Shimizu, F. Iga, and T. Takabatake, *Phys. Rev. Lett.* **82**, 992 (1999).

²⁷T. Susaki, A. Sekiyama, K. Kobayashi, T. Mizokawa, A. Fujimori, M. Tsunekawa, T. Muro, T. Matsushita, S. Suga, H. Ishii, T. Hanyu, H. Namatame, M. Taniguchi, J. Miyahara, F. Iga, M. Kasaya, and H. Harima, *Phys. Rev. Lett.* **77**, 4269 (1996).

²⁸H. Okamura, S. Kimura, H. Shinozaki, T. Nanba, F. Iga, N. Shimizu, and T. Takabatake, *Phys. Rev. B* **58**, R7496 (1998).

²⁹F. Iga, Y. Takakuwa, T. Takahashi, M. Kasuya, T. Kasuya, and T. Sagawa, *Solid State Commun.* **50**, 903 (1984).

³⁰A. Yanase and H. Harima, *Prog. Theor. Phys. Suppl.* **108**, 19 (1992).

³¹V. N. Antonov, B. N. Harmon, and A. N. Yaresko, *Phys. Rev. B* **66**, 125208 (2002).

³²P. Villars and L. D. Calvert, *Pearson's Handbook of Crystallographic Data for Intermetallic Phases* (ASM International, Materials Park, 1991).

³³L. L. Hirst, *Phys. Kondens. Mater.* **11**, 255 (1970).

- ³⁴C. M. Varma, *Rev. Mod. Phys.* **48**, 219 (1976).
- ³⁵V. N. Antonov, A. N. Yaresko, A. Ya. Perlov, P. Thalmeier, P. Fulde, P. M. Oppeneer, and H. Eschrig, *Phys. Rev. B* **58**, 5043 (1998).
- ³⁶V. N. Antonov, B. N. Harmon, V. P. Antropov, A. Ya. Perlov, and A. N. Yaresko, *Phys. Rev. B* **64**, 134410 (2001).
- ³⁷F. Gerken, *J. Phys. F: Met. Phys.* **13**, 703 (1983).
- ³⁸E. Kierzek-Pecold, *Phys. Status Solidi* **33**, 523 (1969).
- ³⁹S. Kimura, T. Nanba, S. Kunii, and T. Kasuya, *J. Phys. Soc. Jpn.* **59**, 3388 (1990).
- ⁴⁰S. Kimura, T. Nanba, T. Tomikawa S. Kunii, and T. Kasuya, *Phys. Rev. B* **46**, 12 196 (1992).
- ⁴¹T. Nanba, H. Ohta, M. Motokawa, S. Kimura, S. Kunii, and T. Kasuya, *Physica B* **188**, 440 (1993).
- ⁴²S. Kimura, T. Nanba, S. Kunii, and T. Kasuya, *Phys. Rev. B* **50**, 1406 (1994).
- ⁴³S. Curnoe and K. A. Kikoin, *Phys. Rev. B* **61**, 15 714 (2000).
- ⁴⁴T. Kasuya, *J. Phys. Colloq.* **37**, C4 (1976); T. Kasuya, K. Takegahara, and T. Fujita, *ibid.* **40**, C5 (1979); **40**, 308 (1979); T. Kasuya, *Europhys. Lett.* **26**, 277 (1994).
- ⁴⁵H. S. Bennet and E. A. Stern, *Phys. Rev.* **137**, A448 (1965).
- ⁴⁶Additional support of the idea that the 4 peak structure of the XPS in YbB_{12} is due to surface effects can be found from recent measurements by S. Suga, A. Sekiyama, S. Imada, A. Yamasaki, F. Iga, T. Takabatake, T. Ebihara, Y. Onuki, and Y. Saitoh, Poster II-98 in The International Conference on Strongly Correlated Electron Systems, August 6–10, Ann Arbor, 2001 (unpublished). They show that YbB_{12} high resolution photoemission spectra have a tendency toward 2 peaks structure when surface defects decreased.